Article:
Qiu, Z, Song, H, Hu, C et al. (2 more authors) (2019) Carbonate thermoluminescence and its implication for marine productivity change during the Permian-Triassic transition. Palaeogeography, Palaeoclimatology, Palaeoecology, 526. pp. 72-79. ISSN 0031-0182

https://doi.org/10.1016/j.palaeo.2019.04.021

Carbonate thermoluminescence and its implication for marine productivity change during the Permian-Triassic transition

Zhipu Qiu[a], Haijun Song[a,*], Chaoyong Hu[a,*], Paul B. Wignall[b], Huyue Song[a]

[a] State Key Laboratory of Biogeology and Environmental Geology, School of Earth Sciences, China University of Geosciences, Wuhan 430074, China

[b] School of Earth and Environment, University of Leeds, Leeds LS2 9JT, UK.

* Corresponding authors.

E-mail addresses: haijunsong@cug.edu.cn (H. Song), chyhu@cug.edu.cn (C. Hu).

Abstract

The Permian-Triassic (P-Tr) crisis was the largest mass extinction of the Phanerozoic and eliminated over 90% of marine species. However, the nature of marine productivity changes during the crisis is a matter of on-going debate. Here, thermoluminescence (TL) measurements from 144 bulk carbonate samples from Meishan (South China) show two levels of variation in TL peak intensities at ~270°C. The first-order variation is characterized by a rapid, nearly three-fold increase. A secondary variation is interpreted to record periodic fluctuations on a Milankovitch scale (~20-kyr rhythm). The periodic variations of TL are negatively correlated with Mn concentrations, suggesting primary productivity is a key factor controlling the TL peak intensity by photo-reduction of

particulate Mn in the presence of organic matter. Therefore, the periodic fluctuations of TL were likely controlled by primary productivity changes on orbital timescales. A significant rise of TL peak intensities across the P-Tr boundary represents the rapid increase of dissolved Mn associated with enhanced marine productivity and/or oceanic anoxia.

Keywords:

Meishan section, Permian-Triassic extinction, dissolved Mn, Milankovitch cycle, carbon isotope, oceanic anoxia

1. Introduction

The Permian-Triassic (P-Tr) mass extinction was the largest crisis of the Phanerozoic with ~90% of marine species lost (e.g., Erwin, 1993; Song et al., 2013b). Biodiversity of marine invertebrates was dramatically reduced and remained low during the Early Triassic (Alroy et al., 2008). However, primary productivity changes during this extinction event and its aftermath are poorly understood. Both the low- and high-productivity levels have been advocated for the Early Triassic oceans. Purported evidence for low-productivity levels, includes a decrease in fossil abundance (Twitchett, 2001), a reduction in fossil size (Twitchett, 2007; He et al., 2015), and negative excursion in marine carbonate $\delta^{13}C$ values (Rampino and Caldeira, 2005). Alternatively, high-productivity has been invoked with supporting evidence including enhanced carbon isotope depth gradients (Meyer et al., 2011; Song et al., 2012a; Song et al., 2013a), the development of organic-rich mudstones (Suzuki et al., 1998), increased burial fluxes of organic carbon (Algeo et al., 2013; Shen et al., 2015), cyanobacteria blooms (Xie et al., 2007).

Dissolved Mn in shallow water is influenced by biochemical processes, which are linked to primary productivity. A typical dissolved Mn profile shows a maximum concentration in the surface due to the photochemical reduction of particulate Mn in the presence of dissolved organic substances, such as humic acid (Sunda et al., 1983; Sunda and Huntsman, 1994). This photochemical reduction effect is amplified as dissolved organic matter concentration increases in more productive waters, resulting in an increase of dissolved Mn. Dissolved Mn in seawater can substitute in calcite lattices, although it is restricted by the distribution coefficient (Dromgoole and Walter, 1990). However, it is very difficult to measure the Mn content in calcite because it is hard to distinguish Mn substituted in calcite lattices from rhodochrosite ($MnCO_3$). In addition, exchangeable Mn^{2+} absorbed by clays also interferes with the results. Although $MgCl_2$ and $CaCl_2$ have been used to extract exchangeable metals (e.g., Poulton and Canfield, 2005), it is difficult to confirm that the exchangeable Mn^{2+} has been completely removed.

Thermoluminescence (TL) in calcite is usually associated with the presence of Mn^{2+} substituted in calcite lattices (Medlin, 1959; Calderón et al., 1996). TL is the thermally stimulated emission of light following the previous absorption of energy on electrons trapped in mineral lattices from electromagnetic or ionizing radiation (Bos, 2006). Thus, TL from carbonate samples, which have been radiated enough to make energy storage electrons reach a saturated state, is related to the crystal lattice properties. The intensity of the ~270°C peak has been reported to be linear with Mn^{2+} concentrations, as Mn^{2+} is considered as the isolated activator center for calcites (Medlin, 1968; Calderón et al., 1996; Polikreti et al., 2003). Unfortunately, Fe^{3+}, Co^{2+} and Ni^{2+} can act as effective poisoners for Mn luminescence (Medlin, 1959, 1968). Usually, Co and Ni concentrations in limestones are less than 100 ppm and almost two orders of

magnitude lower than those of Fe and Mn (Graf, 1960). Iron is preferably present in the soluble divalent state in the ocean and has no quenching effect unless in the presence of SO_4^{2-} or PO_4^{3-} (Medlin, 1959). Iron is an essential element and is present in low concentrations in the surface layer as a result of the uptake by plankton (Morel and Price, 2003; Boyd and Ellwood, 2010), resulting in concentrations that are an order magnitude lower than Mn concentrations in both oxic and anoxic oceans, e.g., the northern Pacific Ocean (Landing and Bruland, 1980; Martin and Michael Gordon, 1988), the eastern Atlantic Ocean (Statham et al., 1998), the Black Sea (Haraldsson and Westerlund, 1988; Lewis and Landing, 1991), and the Framvaren Fjord (Haraldsson and Westerlund, 1988; Yao and Millero, 1995).. Therefore, the quenching effect of Fe^{2+} on calcite is possibly weak. Therefore, the intensities of the ~270°C peak of carbonate samples are usually controlled by Mn substituted in calcite lattices. This is supported by experimental studies that show dissolved Mn in waters has a positive relationship with Mn substituted in precipitated calcite (Fujiwara, 1964; Polikreti et al., 2003). Thus, with provisos, carbonate TL, provides a proxy of the Mn content in calcite and a means of assessing the original dissolved Mn variations in seawater. In this study, high-resolution carbonate TL data, together with isotopic and elemental measurements from the Meishan section (global stratotype section and point, GSSP of the P-Tr boundary), are used to examine changes of primary productivity during the P-Tr transition.

2. Geological setting

We measured the TL of carbonates from the Meishan section, the Global Stratotype Section and Point (GSSP) of the Permian-Triassic boundary (Yin et al., 2001). The ~1.4 m thickness of strata from Beds 24−30 contains six conodont zones (*Clarkina yini* Zone (Bed 24), *C.*

meishanensis Zone (Beds 25), *Hindeodus changxingensis* Zone (Beds 27a−b), *H. parvus* Zone (Bed 27c), *Isarcicella staeschei* Zone (Beds 27d−28) and *I. isarcica* Zone (Beds 29 and above); Yin et al., 2001; Jiang et al., 2007) of approximately 240 thousand years duration (Wu et al., 2013; Burgess et al., 2014). The P-Tr boundary is defined by the first occurrence of *Hindeodus parvus* at the base of Bed 27c (Yin et al., 2001; Jiang et al., 2007). The strata near the P-Tr boundary were deposited on the northeastern slope margin of Yangtze Platform in the eastern part of Paleotethys near the paleoequator (Fig. 1).

3. Methods

Thin-sections were obtained from a selection of samples, in order to undertake petrographic analysis of the sediments and to observe any diagenetic alteration of the samples. Cathodoluminescence (CL) microscopy was performed on CL8200MK5 cold-cathode luminescence device mounted on a Leica DM2500P Polarization Microscope equipped with a Leica DFC300FX digital camera. Operating voltages were 20 kV and gun current levels were 312 μA.

Thermoluminescence and geochemical analyses were performed in the State Key Laboratory of Biogeology and Environment Geology, China University of Geosciences (Wuhan). A total of 144 carbonate samples, without calcite veins, were selected, ground and trimmed prior to powdering (200 mesh), and subsequently naturally dried. Before TL measurements, all samples were gamma-irradiated in the laboratory with a dose of 20 kGy so that energy reach a saturated state. The TL measurements were performed with RGD-3B thermoluminescence dosimeter (TLD). The samples were heated at rate of 5°C/s from 50°C to 400°C under a CO_2 atmosphere.

The instrument sensitivity was set to 5.4. The experimental data was divided by the percentage content of calcium and magnesium to get the final data.

Element abundances (Ca, Mg, Mn, and Sr) were obtained from the same powdered samples. Each sample (5 ± 0.3 mg) was adequately dissolved in 10 mL 1% nitric acid, and then filtered to remove insoluble substances. The diluted solution was measured by IRIS Intrepid II XSP in the State Key Laboratory of Biogeology and Environment Geology, China University of Geosciences (Wuhan). Analytical precision was better than ±5‰.

Carbon and oxygen isotopic analyses were performed at the State Key Laboratory of Biogeology and Environmental Geology of the China University of Geosciences (Wuhan). Each powdered sample (150−400 μg) was placed in a 10 mL Na-glass vial, sealed with a butyl rubber septum, and reacted with 100% phosphoric acid at 72°C after flushing with helium. The evolved CO_2 gas was analyzed for $\delta^{13}C$ and $\delta^{18}O$ using a MAT 253 mass-spectrometer coupled directly to a Finnigan Gasbench II interface (Thermo Scientific). Analytical precision was better than ±0.1‰ for both $\delta^{13}C$ and $\delta^{18}O$ based on replicate analyses of two Chinese national standards (GBW 04416: $\delta^{13}C$ = +1.61‰, $\delta^{18}O$ = −11.59‰; GBW 04417: $\delta^{13}C$ = −6.06‰, $\delta^{18}O$ = −24.12‰). All the values are reported in the per mil notation relative to the Vienna Pee Dee Belemnite (VPDB) standard.

4. Results

Bed 24, the top unit of the Changxing Formation, is formed of bioclastic packstone with microsparite and sparry calcite matrix (Fig. 4A). The matrix in Bed 24 is non-luminescence to dull-orange luminescence (Fig. 4B). Bed 27 comprises biotic wackestone with microsparite,

micrite matrix (Fig. 4C). The matrix in Bed 27 is dull-orange luminescence (Fig. 4D). Beds 29 and 30 are marlstone with micrite matrix and lacks any fossil fragments (Fig. 4E). Micritic matrix shows bright-orange luminescence (Fig. 4F). The typical glow curve of carbonate is given in figure 2. The TL data, as well as carbon isotope and Mn concentrations from the P-Tr boundary strata, are illustrated in figure 3 and Table S1. The TL peak intensities at ~270°C are normalized by carbonate ($CaCO_3$ + $MgCO_3$) molar contents. The curve of TL peak intensity shows a rapid, increasing trend and a prominent periodic variation from Beds 24 to 30. It averages ~12400 arbitrary unit/mol (a.u./mol) in Bed 24 and increases by ~21820 a.u./mol across the main extinction horizon (Beds 25 and 26) and fluctuates around ~36170 a.u./mol in Bed 27. The TL curve shows an overall increase from ~30,000 to ~60,000 a.u./mol in Beds 29 and 30. Wavelet analysis shows that the secondary variations in TL data are characterized by a periodic feature, which accords with the ~20-thousand years (kyr) filter (Fig. 3).

The curve of Mn concentrations shows a similar increase during the P-Tr transition and periodic variations from Beds 24 to 30 (Fig. 3). Mn concentration is approximately 100 ppm in the lower and middle parts of Bed 24 and increases above this level, reaching up to 1200 ppm at the top of Bed 29. This is followed by a rapid decrease from 1200 ppm to ~550 ppm in Bed 30.

The $\delta^{13}C$ values of carbonate rocks exhibits a decline across the P-Tr boundary. They range from 0.04 to 3.36‰ VPDB in Bed 24 with a weak periodicity (Fig. 3). Samples from Bed 27 show an obvious variation in $\delta^{13}C$ values from −1.29 to 1.34‰ VPDB. In Beds 29 to 30, there is little variation in $\delta^{13}C$ values from 0.51 to 1.46‰ VPDB.

5 Discussion

149 ***5.1. Preservation of primary TL signatures***

150 Two major factors influence the TL peak intensities of carbonates: (1) number of electronic
151 trapping centers (crystal defects) in the carbonate lattices, which form during the process of
152 crystallization of carbonate minerals, and (2) environmental radiation from rays generated by the
153 decay of radioelements (e.g., U and K) around. With longer radiated time and higher radiant
154 intensity, the number of energy storage electrons in crystal lattices would increase and emit a
155 stronger TL. For carbonate samples from the P-Tr boundary interval, all of them have been
156 gamma-irradiated in the laboratory with a dose of 20 kGy to ensure the energy has reached a
157 saturated state, and thus the environmental radiation is unlikely to have influenced TL peak
158 intensity variations. Therefore, the major factor influencing the TL peak intensities of carbonates
159 from the P-Tr strata is the number of electronic trapping centers in carbonate, which is related to
160 the type and concentration of impurity ions (e.g., Mn^{2+} and Fe^{3+}) doped in carbonate (Medlin,
161 1959, 1968).

162 Diagenesis can change the chemical composition and lattice properties of carbonate
163 components (Brand and Veizer, 1980, 1981; Algeo et al., 1992), which can alter the primary TL
164 signatures. During diagenetic stabilization with meteoric waters, Mn may be incorporated and Sr
165 may be expelled from the carbonate system (Brand and Veizer, 1980). It is generally accepted
166 that Mn^{2+} is the most important activators of extrinsic CL in carbonate minerals (yellow-orange
167 CL for calcite and yellow-red CL for dolomite) (Richter et al., 2003). Therefore, carbonates with
168 bright-orange CL in Beds 27, 29 and 30 possibly contain more Mn ions than that in Bed 24.
169 Besides, the carbonate rocks with Mn/Sr ratios less than 2 were generally not subjected to
170 significant diagenesis (Jacobsen and Kaufman, 1999). Samples in Bed 24 with low Mn/Sr ratios

(0.02−1.95, Table S1) possibly indicate minor diagenetic alteration. Although samples in Beds 27, 29 and 30 have high Mn/Sr ratios (1.80−5.47, Table S1), there is poor negative covariance between Mn/Ca and Sr/Ca in each bed (Fig. 4A). This is likely the result of the transitions from limestone (Bed 24) to muddy limestone (Beds 27, 29 and 30).

In addition, a positive correlation between $\delta^{13}C$ and $\delta^{18}O$ in Beds 27, 29, and 30 is presented in our data. This correspondence is generally thought to be caused by meteoric diagenesis (Brand and Veizer, 1981). However, such an analysis might not be valid in this case because our samples are positioned in a region of the $\delta^{13}C$ and $\delta^{18}O$ cross-plot (Fig. 5B) that is not typical for carbonate rock subjected to meteoric diagenesis (Knauth and Kennedy, 2009). This region is thought to be experienced later deep burial and/or metamorphic alteration (shown by the red arrow in Fig. 5B; Knauth and Kennedy, 2009). Besides, the carbonate succession in the Meishan section is generally considered to have accumulated on a carbonate slope in water ~100−200 m deep with no indications of subaerial exposure (Zheng et al., 2013).

To sum up, samples in Bed 24 may preserve the primary TL signature with minor diagenetic alteration. Although samples in Beds 27, 29, 30 were subjected to potential diagenesis, the significant periodic variations of carbonate TL peak intensities are not altered. These periodic variations accord with the ~20-kyr (~10 cm thick strata) filter (see Fig. 3). If the increase of carbonate TL peak intensities were principally triggered by diagenesis, such minor periodic fluctuations can hardly be retained.

5.2 Periodic variations of TL peak intensities associated with orbital forcing

As shown in figure 3, a prominent periodic variation is seen in the TL peak intensities, which

is almost consistent with the magnetic susceptibility, and possibly accords with the Milankovitch-band 20-kyr precession cycle (Wu et al., 2013). Although the periodic variation of carbon isotope is not as clearly seen as in the TL data, it is likely coincident with both TL peak intensity and magnetic susceptibility to a certain extent as shown by black arrows (Fig. 3). However, Mn concentrations of bulk samples show obvious inverted variations with the TL peak intensities. Both intervals below and above the main extinction horizon (Bed 25 at Meishan, see Song et al., 2013b) see a negative relationship between Mn concentrations and TL peak intensities in Bed 24 ($n = 80$, $r = -0.39$, $p < 0.01$) and Beds 27−30 ($n = 64$, $r = -0.56$, $p < 0.01$) (Fig. 6).

The negative relationship between TL peak intensities and Mn concentrations demonstrates that TL peak intensities can reflect dissolved Mn in paleo-ocean, and likely result from the periodic change of primary productivity on orbital timescales. Increased primary productivity can enhance the photo-reduction of particulate Mn in shallow water, because the reduction depends on organic matter (Sunda et al., 1983; Sunda and Huntsman, 1994). In addition, more organic matter would consume dissolved oxygen and result in relatively reducing environments. As a result, dissolved Mn concentration increased while particulate Mn concentration decreased in shallow water. Finally, carbonate TL peak intensities elevate due to higher Mn content substituted in calcite lattices, but total Mn concentrations possibly reduce on account of lower particulate Mn concentrations. This process can also be linked to carbon isotope fluctuations. As shown by black arrows in Fig. 3, higher $\delta^{13}C$ values correspond to increased carbonate TL peak intensities in Beds 24, 27 and 29. A similar ~20-kyr periodicity of carbon isotopes was detected in planktonic foraminifers of Late Quaternary age (Schneider et al., 1994), possibly due to

214 precessional-scale variation of upwelling intensity. Because of depleted ^{13}C in organic carbon,
215 high primary productivity can increase the $\delta^{13}C$ value of dissolved inorganic carbon.

216 The second-order variation of TL peak intensities is negatively correlated with Mn contents,
217 but the first-order variation especially the rapid increase across the P-Tr boundary accompanies
218 with the increase of total Mn contents. This phenomenon is possibly due to lithological variation
219 at the transitions from limestone (Bed 24) to muddy limestone (Beds 27, 29 and 30), perhaps
220 driven by enhanced continental weathering (Algeo and Twitchett, 2010; Song et al., 2015).
221 Lithological variation can effectively change Mn contents, but have little influence on carbonate
222 TL. In addition, a negative excursion in carbonate $\delta^{13}C$ occurred during the P-Tr transition. This
223 may be due to release of volcanic CO_2 from the Siberian Trap volcanism (Wignall, 2001;
224 Reichow et al., 2002; Vyssotski et al., 2006; Korte and Kozur, 2010), and methane from thermal
225 metamorphism of organic-rich sediments by igneous intrusion (Korte and Kozur, 2010; Burgess
226 et al., 2017).

227 ***5.3 Increased TL peak intensities and their implication for primary productivity change***

228 The three-fold increase of carbonate TL peak intensity from 12410 to 34320 a.u./mol across
229 the P-Tr boundary is likely a result of increased dissolved Mn in shallow water. In modern ocean,
230 Mn ions is lost from the water column via scavenging and sinking of particulate Mn oxides
231 (Sunda and Huntsman, 1994). This is observed below the photic zone, where dissolved Mn
232 concentrations decrease quickly with increasing depth to low uniform concentrations (~0.15
233 nmol/L in deep ocean) (Landing and Bruland, 1980; Statham et al., 1998). However, in the
234 surface layer a typical dissolved Mn profile shows elevated concentrations (e.g., Landing and

Bruland, 1980) due to the photo-reduction of particulate Mn in the presence of dissolved organic substances, such as humic acid (Sunda et al., 1983; Sunda and Huntsman, 1994). Therefore, in the P-Tr ocean, widespread oceanic anoxia, even in the photic zone, (Wignall and Twitchett, 1996; Grice et al., 2005; Kaiho et al., 2012; Song et al., 2012b) might contribute to increased dissolved Mn in shallow water. In addition, increased dissolved Mn also suggests higher primary productivity, that would have led to elevated photo-reduction of particulate Mn.

Higher productivity after the P-Tr boundary crisis is also supported by other proxies (Fig. 7). Enhanced continental weathering (Algeo and Twitchett, 2010; Winguth and Winguth, 2012; Song et al., 2015) may have played a key role in the increase of marine productivity during the P-Tr transition. The increased terrigenous run-off would also supply more nutrients to the oceans (Algeo and Twitchett, 2010; Winguth and Winguth, 2012; Song et al., 2015), which would fertilized the Early Triassic oceans. As a result, primary producers, e.g., cyanobacteria and green sulfur bacteria, bloomed in the Early Triassic ocean (Grice et al., 2005; Xie et al., 2007), generated a vigorous biological pump (Meyer et al., 2011; Song et al., 2012a; Song et al., 2013a).

Evidence for low primary productivity, such as decreased in fossil abundance (Twitchett, 2001) and smaller fossils (Twitchett, 2007) can alternatively be explained as a response to harsh environmental conditions independent of productivity changes, e.g., ocean anoxia (Wignall and Twitchett, 1996; Grice et al., 2005; Kaiho et al., 2012; Song et al., 2012b) and global warming (Joachimski et al., 2012; Sun et al., 2012). Furthermore, species in eutrophic environments are often '*r*-strategists' which are often small and show rapid growth and onset of sexual maturity (Pianka, 1970).

6 Conclusions

High-resolution TL measurements based on 144 carbonate samples of GSSP Meishan section show that carbonate TL peak intensity at ~270°C is characterized by two features during the P-Tr transition, periodic variations and a long-term rapid increase. The former span the Late Permian to Early Triassic and accord with a Milankovitch-band ~20-kyr rhythm. The rapid rise occurs at the latest Permian extinction horizon, and shows values rise nearly threefold. The periodic variations of TL peak intensities are negatively correlated with Mn concentrations, possibly caused by primary productivity change at orbital timescales. Increased primary productivity can provide more organic matter for photo-reduction of particulate Mn in shallow water. As a result, carbonate TL peak intensities elevate due to higher dissolved Mn concentration, but total Mn concentrations of samples possibly reduce on account of lower particulate Mn concentrations. The rapid rise of TL peak intensity across the P-Tr boundary potentially records increased photo-reduction of particulate Mn due to higher primary productivity and/or enhanced reduction of Mn oxides under anoxic environments.

Acknowledgments

This study is supported by the National Natural Science Foundation of China (41622207, 41821001, 41731177, 41661134047), the State Key R&D project of China (2016YFA0601100), the Strategic Priority Research Program of Chinese Academy of Sciences (XDB26000000), and the Natural Environment Research Council's Eco-PT project (NE/P0137224/1), which is a part of the Biosphere Evolution, Transitions and Resilience Program (BETR). This study is a contribution to the IGCP 630 project.

References

Abdel-Razek, Y.A., 2016. Thermoluminescence dosimetry using natural calcite. J. Taibah Univ. Sci. 10, 286−295, https://doi.org/10.1016/j.jtusci.2015.08.002.

Algeo, T.J., Henderson, C.M., Tong, J., Feng, Q., Yin, H., Tyson, R.V., 2013. Plankton and productivity during the Permian–Triassic boundary crisis: an analysis of organic carbon fluxes. Glob. Planet. Change 105, 52−67, https://doi.org/10.1016/j.gloplacha.2012.02.008.

Algeo, T.J., Twitchett, R.J., 2010. Anomalous Early Triassic sediment fluxes due to elevated weathering rates and their biological consequences. Geology 38, 1023−1026, https://doi.org/10.1130/G31203.1.

Algeo, T.J., Wilkinson, B.H., Lohmann, K.C., 1992. Meteoric-burial diagenesis of Middle Pennsylvanian limestones in the Orogrande Basin, New Mexico; water/rock interactions and basin geothermics. J. Sediment. Res. 62, 652−670, https://doi.org/10.1306/D426797E-2B26-11D7-8648000102C1865D.

Alroy, J., Aberhan, M., Bottjer, D.J., Foote, M., Fürsich, F.T., Harries, P.J., Hendy, A.J., Holland, S.M., Ivany, L.C., Kiessling, W., 2008. Phanerozoic trends in the global diversity of marine invertebrates. Science 321, 97−100, https://doi.org/10.1126/science.1156963.

Baı¨etto, V., Villeneuve, G., Guibert, P., Schvoerer, M., 2000. EPR and TL correlation in some powdered Greek white marbles. Appl. Radiat. Isot. 52, 229−235, https://doi.org/10.1016/S0969-8043(99)00120-7.

Bos, A., 2006. Theory of thermoluminescence. Radiat. Meas. 41, S45−S56, https://doi.org/10.1016/j.radmeas.2007.01.003.

Boyd, P.W., Ellwood, M.J., 2010. The biogeochemical cycle of iron in the ocean. Nat. Geosci. 3, 675−682 , https://doi.org/10.1038/ngeo964.

Brand, U., Veizer, J., 1980. Chemical diagenesis of a multicomponent carbonate system; 1, Trace elements. J. Sediment. Res. 50, 1219−1236, https://doi.org/10.1306/212F7BB7-2B24-11D7-8648000102C1865D.

Brand, U., Veizer, J., 1981. Chemical diagenesis of a multicomponent carbonate system; 2, Stable isotopes. J. Sediment. Res. 51, 987−997, https://doi.org/10.1306/212F7DF6-2B24-11D7-8648000102C1865D.

Bruce, J., Galloway, R.B., Harper, K., Spink, E., 1999. Bleaching and phototransfer of thermoluminescence in limestone. Radiat. Meas. 30, 497−504, https://doi.org/10.1016/S1350-4487(99)00208-5.

Burgess, S.D., Bowring, S., Shen, S.-z., 2014. High-precision timeline for Earth's most severe extinction. Proc. Natl. Acad. Sci. 111, 3316−3321, https://doi.org/10.1073/pnas.1317692111.

Burgess, S.D., Muirhead, J.D., Bowring, S.A., 2017. Initial pulse of Siberian Traps sills as the trigger of the end-Permian mass extinction. Nat. Commun. 8, 164, https://doi.org/10.1038/s41467-017-00083-9.

Calderón, T., Townsend, P.D., Beneitez, P., Garcia-Guinea, J., Millán, A., Rendell, H.M., Tookey, A., Urbina, M., Wood, R.A., 1996. Crystal field effects on the thermoluminescence of manganese in carbonate lattices. Radiat. Meas 26, 719−731, https://doi.org/10.1016/S1350-4487(97)82886-7.

Dromgoole, E.L., Walter, L.M., 1990. Iron and manganese incorporation into calcite: Effects of growth kinetics, temperature and solution chemistry. Chem. Geol. 81, 311−336, https://doi.org/10.1016/0009-2541(90)90053-A.

Erwin, D.H., 1993. The Great Paleozoic Crisis: Life and Death in the Permian. Columbia University Press, New York.

Feng, Z., Bao, Z., Liu, S., 1997. Lithofacies Palaeogeography of Early and Middle Triassic of South China. Petroleum Industry Press, Beijing.

Fujiwara, S., 1964. Investigation of Trace Impurities in Solids by Electron Paramagnetic Resonance. Distribution of Manganese in Calcium Carbonate. Analytical Chemistry 36, 2259−2261, https://doi.org/10.1021/ac60218a012.

Graf, D.L., 1960. Geochemistry of Carbonate Sediments and Sedimentary Carbonate Rocks: pt. III, Minor Element Eistribution. Illinois State Geological Survey Circular 301.

Grice, K., Cao, C., Love, G.D., Bottcher, M.E., Twitchett, R.J., Grosjean, E., Summons, R.E., Turgeon, S.C., Dunning, W., Jin, Y., 2005. Photic Zone Euxinia During the Permian-Triassic Superanoxic Event. Science 307, 706−709, https://doi.org/10.1126/science.1104323.

Haraldsson, C., Westerlund, S., 1988. Trace metals in the water columns of the Black Sea and Framvaren Fjord. Mar. Chem. 23, 417−424, https://doi.org/10.1016/0304-4203(88)90108-9.

He, W.H., Shi, G., Twitchett, R., Zhang, Y., Zhang, K.X., Song, H.J., Yue, M.L., Wu, S.B., Wu, H.T., Yang, T.L., 2015. Late Permian marine ecosystem collapse began in deeper waters: evidence from brachiopod diversity and body size changes. Geobiology 13, 123−138, https://doi.org/10.1111/gbi.12119.

Jacobsen, S.B., Kaufman, A.J., 1999. The Sr, C and O isotopic evolution of Neoproterozoic seawater. Chem. Geol. 161, 37−57, https://doi.org/10.1016/S0009-2541(99)00080-7.

Jiang, H., Lai, X., Luo, G., Aldridge, R., Zhang, K., Wignall, P., 2007. Restudy of conodont zonation and evolution across the P/T boundary at Meishan section, Changxing, Zhejiang, China. Glob. Planet. Change 55, 39−55, https://doi.org/10.1016/j.gloplacha.2006.06.007.

Joachimski, M.M., Lai, X., Shen, S., Jiang, H., Luo, G., Chen, B., Chen, J., Sun, Y., 2012. Climate warming in the latest Permian and the Permian–Triassic mass extinction. Geology 40, 195−198, https://doi.org/10.1130/G32707.1.

Kaiho, K., Oba, M., Fukuda, Y., Ito, K., Ariyoshi, S., Gorjan, P., Riu, Y., Takahashi, S., Chen, Z.-Q., Tong, J., Yamakita, S., 2012. Changes in depth-transect redox conditions spanning the end-Permian mass extinction and their impact on the marine extinction: Evidence from biomarkers and sulfur isotopes. Glob. Planet. Change 94-95, 20-32, https://doi.org/10.1016/j.gloplacha.2012.05.024.

Knauth, L.P., Kennedy, M.J., 2009. The late Precambrian greening of the Earth. Nature 460, 728−732, https://doi.org/10.1038/nature08213.

Korte, C., Kozur, H.W., 2010. Carbon-isotope stratigraphy across the Permian–Triassic boundary: A review. J. Asian Earth Sci. 39, 215−235, https://doi.org/10.1016/j.jseaes.2010.01.005.

Landing, W.M., Bruland, K.W., 1980. Manganese in the North Pacific. Earth Planet. Sci. Lett. 49, 45−56, https://doi.org/ 10.1016/0012-821X(80)90149-1.

Lehrmann, D.J., Wei, J., Enos, P., 1998. Controls on facies architecture of a large Triassic carbonate platform: the Great Bank of Guizhou, Nanpanjiang Basin, South China. J. Sediment. Res. 68, 311−326, https://doi.org/10.2110/jsr.68.311.

Lewis, B.L., Landing, W.M., 1991. The biogeochemistry of manganese and iron in the Black Sea. Deep-Sea Res., Part A 38, S773−S803, https://doi.org/10.1016/S0198-0149(10)80009-3.

Martin, J.H., Michael Gordon, R., 1988. Northeast Pacific iron distributions in relation to phytoplankton productivity. Deep-Sea Res., Part A 35, 177−196, https://doi.org/10.1016/0198-0149(88)90035-0.

Medlin, W.L., 1959. Thermoluminescent Properties of Calcite. J. Chem. Phys. 30, 451−458, https://doi.org/10.1063/1.1729973.

Medlin, W.L., 1968. The nature of traps and emission centers in thermoluminescent rock materials, in: McDougall, D.J. (Ed.), Thermoluminescence of Geological Materials. Academic Press, London, pp. 193−223.

Meyer, K.M., Yu, M., Jost, A.B., Kelley, B.M., Payne, J.L., 2011. $\delta^{13}C$ evidence that high primary productivity delayed recovery from end-Permian mass extinction. Earth Planet. Sci. Lett. 302, 378−384, https://doi.org/10.1016/j.epsl.2010.12.033.

Morel, F.M.M., Price, N.M., 2003. The Biogeochemical Cycles of Trace Metals in the Oceans. Science 300, 944−947, https://doi.org/10.1126/science.1083545.

Pianka, E.R., 1970. On r-and K-selection. Am. Nat. 104, 592−597, https://doi.org/10.1086/282697.

Polikreti, K., Michael, C.T., Maniatis, Y., 2003. Thermoluminescence characteristics of marble and dating of freshly excavated marble objects. Radiat. Meas. 37, 87−94, https://doi.org/10.1016/S1350-4487(02)00088-4.

Poulton, S.W., Canfield, D.E., 2005. Development of a sequential extraction procedure for iron: implications for iron partitioning in continentally derived particulates. Chem. Geol. 214, 209−221, https://doi.org/10.1016/j.chemgeo.2004.09.003.

Rampino, M.R., Caldeira, K., 2005. Major perturbation of ocean chemistry and a 'Strangelove Ocean' after the end-Permian mass extinction. Terr. Nova 17, 554−559, https://doi.org/10.1111/j.1365-3121.2005.00648.x.

Reichow, M.K., Saunders, A.D., White, R.V., Pringle, M.S., Al'Mukhamedov, A.I., Medvedev, A.I., Kirda, N.P., 2002. 40Ar/39Ar dates from the West Siberian Basin: Siberian flood basalt province doubled. Science 296, 1846−1849, https://doi.org/10.1126/science.1071671.

Richter, D.K., Götte, T., Götze, J., Neuser, R.D., 2003. Progress in application of cathodoluminescence (CL) in sedimentary petrology. Mineral. Petrol. 79, 127−166, https://doi.org/10.1007/s00710-003-0237-4.

Schneider, R.R., Müller, P.J., Wefer, G., 1994. Late Quaternary paleoproductivity changes off the Congo deduced from stable carbon isotopes of planktonic foraminifera. Paleogeogr. Paleoclimatol. Paleoecol. 110, 255−274, https://doi.org/10.1016/0031-0182(94)90087-6.

Scotese, C.R., 2001. Atlas of Earth History, Volume 1, Paleogeography. PALEOMAP Project, University of Texas, Arlington.

Shen, J., Schoepfer, S.D., Feng, Q., Zhou, L., Yu, J., Song, H., Wei, H., Algeo, T.J., 2015. Marine productivity changes during the end-Permian crisis and Early Triassic recovery. Earth-Sci. Rev. 149, 136−162, https://doi.org/10.1016/j.earscirev.2014.11.002.

Song, H., Tong, J., Algeo, T.J., Horacek, M., Qiu, H., Song, H., Tian, L., Chen, Z.-Q., 2013a. Large vertical $\delta^{13}C_{DIC}$ gradients in Early Triassic seas of the South China craton: Implications for oceanographic changes related to Siberian Traps volcanism. Glob. Planet. Change 105, 7−20, https://doi.org/10.1016/j.gloplacha.2012.10.023.

Song, H., Tong, J., Xiong, Y., Sun, D., Tian, L., Song, H., 2012a. The large increase of $\delta^{13}C$ carb-depth gradient and the end-Permian mass extinction. Sci. China Earth Sci. 55, 1101−1109, https://doi.org/10.1007/s11430-012-4416-1.

Song, H., Wignall, P.B., Tong, J., Bond, D.P., Song, H., Lai, X., Zhang, K., Wang, H., Chen, Y., 2012b. Geochemical evidence from bio-apatite for multiple oceanic anoxic events during Permian–Triassic transition and the link with end-Permian extinction and recovery. Earth Planet. Sci. Lett. 353-354, 12−21, https://doi.org/10.1016/j.epsl.2012.07.005.

Song, H., Wignall, P.B., Tong, J., Song, H., Chen, J., Chu, D., Tian, L., Luo, M., Zong, K., Chen, Y., 2015. Integrated Sr isotope variations and global environmental changes through the Late Permian to early Late Triassic. Earth Planet. Sci. Lett. 424, 140−147, https://doi.org/10.1016/j.epsl.2015.05.035.

Song, H., Wignall, P.B., Tong, J., Yin, H., 2013b. Two pulses of extinction during the Permian-Triassic crisis. Nat. Geosci. 6, 52−56, https://doi.org/10.1038/ngeo1649.

Statham, P.J., Yeats, P.A., Landing, W.M., 1998. Manganese in the eastern Atlantic Ocean: processes influencing deep and surface water distributions. Mar. Chem. 61, 55−68, https://doi.org/10.1016/S0304-4203(98)00007-3.

Sun, Y., Joachimski, M.M., Wignall, P.B., Yan, C., Chen, Y., Jiang, H., Wang, L., Lai, X., 2012. Lethally Hot Temperatures During the Early Triassic Greenhouse. Science 338, 366−370, https://doi.org/10.1126/science.1224126.

Sunda, W., Huntsman, S., Harvey, G., 1983. Photoreduction of manganese oxides in seawater and its geochemical and biological implications. Nature 301, 234−236, https://doi.org/10.1038/301234a0.

Sunda, W.G., Huntsman, S.A., 1994. Photoreduction of manganese oxides in seawater. Mar. Chem. 46, 133−152,

https://doi.org/10.1016/0304-4203(94)90051-5.
Suzuki, N., Ishida, K., Shinomiya, Y., Ishiga, H., 1998. High productivity in the earliest Triassic ocean: bl ack shales, Southwest Japan. Paleogeogr. Paleoclimatol. Paleoecol. 141, 53−65, https://doi.org/10.1016/S0 031-0182(98)00009-1.
Twitchett, R.J., 2001. Incompleteness of the Permian–Triassic fossil record: a consequence of productivity decline? Geol. J. 36, 341−353, https://doi.org/10.1002/gj.883.
Twitchett, R.J., 2007. The Lilliput effect in the aftermath of the end-Permian extinction event. Paleogeogr. Paleoclimatol. Paleoecol. 252, 132−144, https://doi.org/10.1016/j.palaeo.2006.11.038.
Vyssotski, A.V., Vyssotski, V.N., Nezhdanov, A.A., 2006. Evolution of the West Siberian Basin. Mar. Pet. Geol. 23, 93−126, https://doi.org/10.1016/j.marpetgeo.2005.03.002.
Wignall, P.B., 2001. Large igneous provinces and mass extinctions. Earth-Sci. Rev. 53, 1−33, https://doi.org/10.1016/S0012-8252(00)00037-4.
Wignall, P.B., Twitchett, R.J., 1996. Oceanic anoxia and the end Permian mass extinction. Science 272, 1155−1158, https://doi.org/10.1126/science.272.5265.1155.
Winguth, C., Winguth, A.M., 2012. Simulating Permian–Triassic oceanic anoxia distribution: implications for species extinction and recovery. Geology 40, 127−130, https://doi.org/10.1130/G32453.1.
Wu, H., Zhang, S., Hinnov, L.A., Jiang, G., Feng, Q., Li, H., Yang, T., 2013. Time-calibrated Milankovitch cycles for the late Permian. Nat. Commun. 4, 2452, https://doi.org/10.1038/ncomms3452.
Xie, S., Pancost, R.D., Huang, J., Wignall, P.B., Yu, J., Tang, X., Chen, L., Huang, X., Lai, X., 2007. Changes in the global carbon cycle occurred as two episodes during the Permian–Triassic crisis. Geology 35, 1083−1086, https://doi.org/10.1130/G24224A.1.
Yao, W., Millero, F.J., 1995. The chemistry of the anoxic waters in the Framvaren Fjord, Norway. Aquat. Geochem. 1, 53−88, https://doi.org/10.1007/bf01025231.
Yin, H., Zhang, K., Tong, J., Yang, Z., Wu, S., 2001. The Global Stratotype Section and Point (GSSP) of the Permian-Triassic Boundary. Episodes 24, 102−114.
Zheng, Q., Cao, C., Zhang, M., 2013. Sedimentary features of the Permian-Triassic boundary sequence of the Meishan section in Changxing County, Zhejiang Province. Sci. China Earth Sci. 56, 956−969, https://doi.org/10.1007/s11430-013-4602-9.

Figure Captions

Fig. 1. Schematic maps of the study area. A. Location map showing the study site, modified from Feng et al. (1997) and Lehrmann et al. (1998). B. Paleogeography illustrating the position of South China during the Permian-Triassic transition, modified from Scotese (2001).

Fig. 2. Typical TL glow curve of the carbonate sample from Meishan Section. Three peaks are generally observed in accord with other researches (Bruce et al., 1999; Polikreti et al., 2003;

444 Abdel-Razek, 2016). The peak at ~170°C is likely produced by laboratory dosed phototransfer
445 (Bruce et al., 1999; Polikreti et al., 2003). Thepeak at ~270°C depends on Mn concentration,
446 because Mn is considered to be the main isolated activator center for calcite (Medlin, 1959;
447 Polikreti et al., 2003). The peak at ~350°C is possibly a spurious signal (Roque et al., 2001) and
448 caused by mechanical treatment (Baı¨etto et al., 2000).

449

450 **Fig. 3.** Profiles of $\delta^{13}C_{carb}$, magnetic susceptibility, Mn concentrations of bulk samples and
451 carbonate TL-peak and wavelet analysis for TL and Mn contents across the P-Tr boundary at
452 Meishan. Magnetic susceptibility values (MS, black solid curve) are from Wu et al. (2013) and
453 the dotted black curve represents the 20- kyr precession cycle (Wu et al., 2013). The U-Pb ages
454 are from Burgess et al. (2014). The dotted pink curve shows the periodic variations in TL-peak
455 after wavelet analysis. The blue dotted curve present wavelet analysis for Mn concentrations.
456 $\delta^{13}C_{carb}$ and TL mostly co-vary with magnetic susceptibility and accord with the ~20- kyr filter.
457

458 **Fig. 4.** Photomicrographs under plane polarized light and CL showing some recrystallization
459 evidence. A. Photomicrograph under plane light of Bed 24 showing grainstone filled with
460 microsparite and sparry calcite matrix. B. Same area as A under CL, showing calcite crystals
461 with dull-orange luminescence. C. Photomicrograph under plane polarized light of Bed 27
462 showing wackestone filled with microsparite and micritic calcite matrix. D. Same area as C
463 under CL, showing matrix with dull-orange luminescence. E. Photomicrograph under plane
464 polarized light of Bed 29 showing wackestone filled with micritic calcite matrix. F. Same area as
465 E under CL showing matrix with bright-orange luminescence.

Fig. 5. Cross plots of (A) Sr/Ca vs Mn/Ca, (B) $\delta^{13}C$ vs $\delta^{18}O$ from Meishan. B also shows the range of Cenozoic carbon and oxygen isotope values from rocks subjected to the influence of either marine or meteoric pore water (Knauth and Kennedy, 2009).

Fig. 6. Cross plots between Mn concentrations and TL. Mn concentrations show a negative relationship with TL in both Bed 24 ($n = 80$, $r = -0.39$, $p < 0.01$) and Beds 27-30 ($n = 64$, $r = -0.56$, $p < 0.01$).

Fig. 7. Comparison of carbonate TL and other paleo-productivity proxies across the P-Tr boundary. A. Decreased $\delta^{13}C$ differences between pristane and phytane and *n*-C17 and *n*-C18 alkanes reflecting increased autotrophs (Grice et al., 2005)) B. C_{31} 2-methylhopane (2-MHP) index interpreted to reflect cyanobacteria proliferation (Xie et al., 2007). C. The $\delta^{13}C_{carb}$-depth gradient suggesting onset of a vigorous biological pump in the late Permian (Song et al., 2012a). D. Carbonate TL peak intensities. *C. m - Clarkina meishanensis, H. chan - Hindeodus changxingensis, H. parv - Hindeodus parvus, I.st - Isarcicella staeschei.*

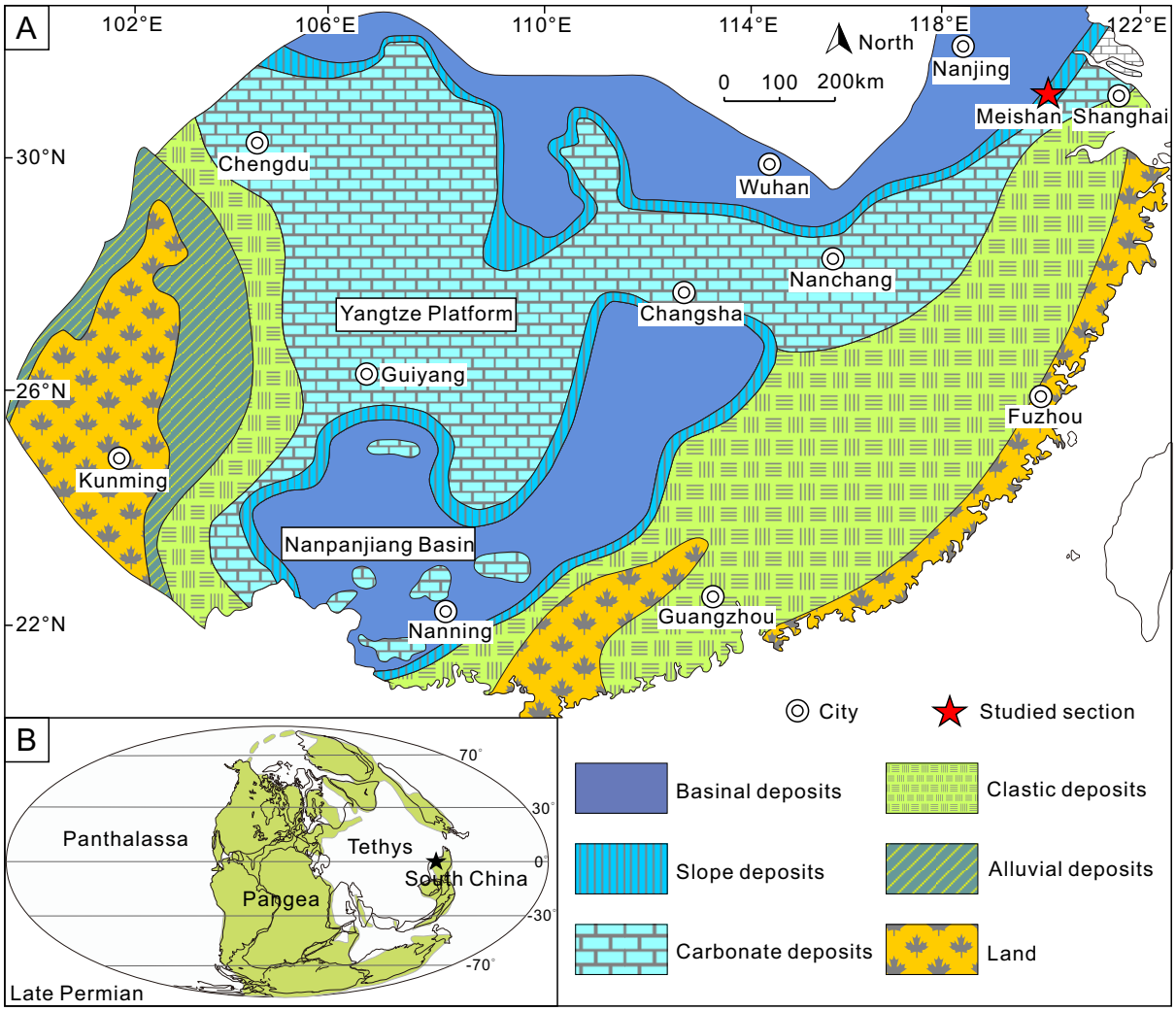
A
102°E
106°E
110°E
114°E
118°E
122°E
North
0 100 200km
30°N
26°N
22°N
Nanjing
Meishan
Shanghai
Chengdu
Wuhan
Nanchang
Changsha
Yangtze Platform
Guiyang
Fuzhou
Kunming
Nanpanjiang Basin
Nanning
Guangzhou
City
Studied section
Basinal deposits
Clastic deposits
Slope deposits
Alluvial deposits
Carbonate deposits
Land
B
70°
30°
0°
-30°
-70°
Panthalassa
Tethys
South China
Pangea
Late Permian

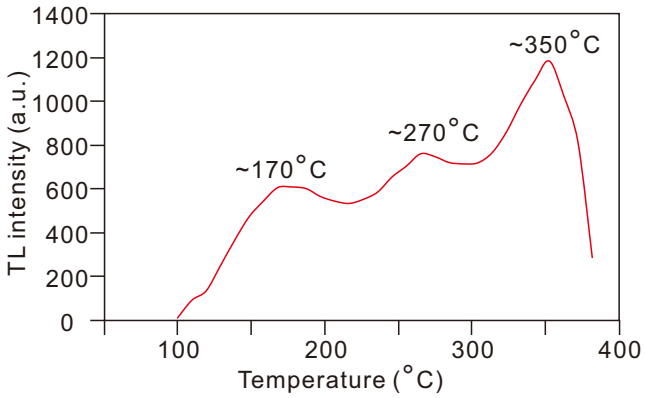
1400
1200
1000
800
600
400
200
0
TL intensity (a.u.)
~170°C
~270°C
~350°C
100
200
300
400
Temperature (°C)

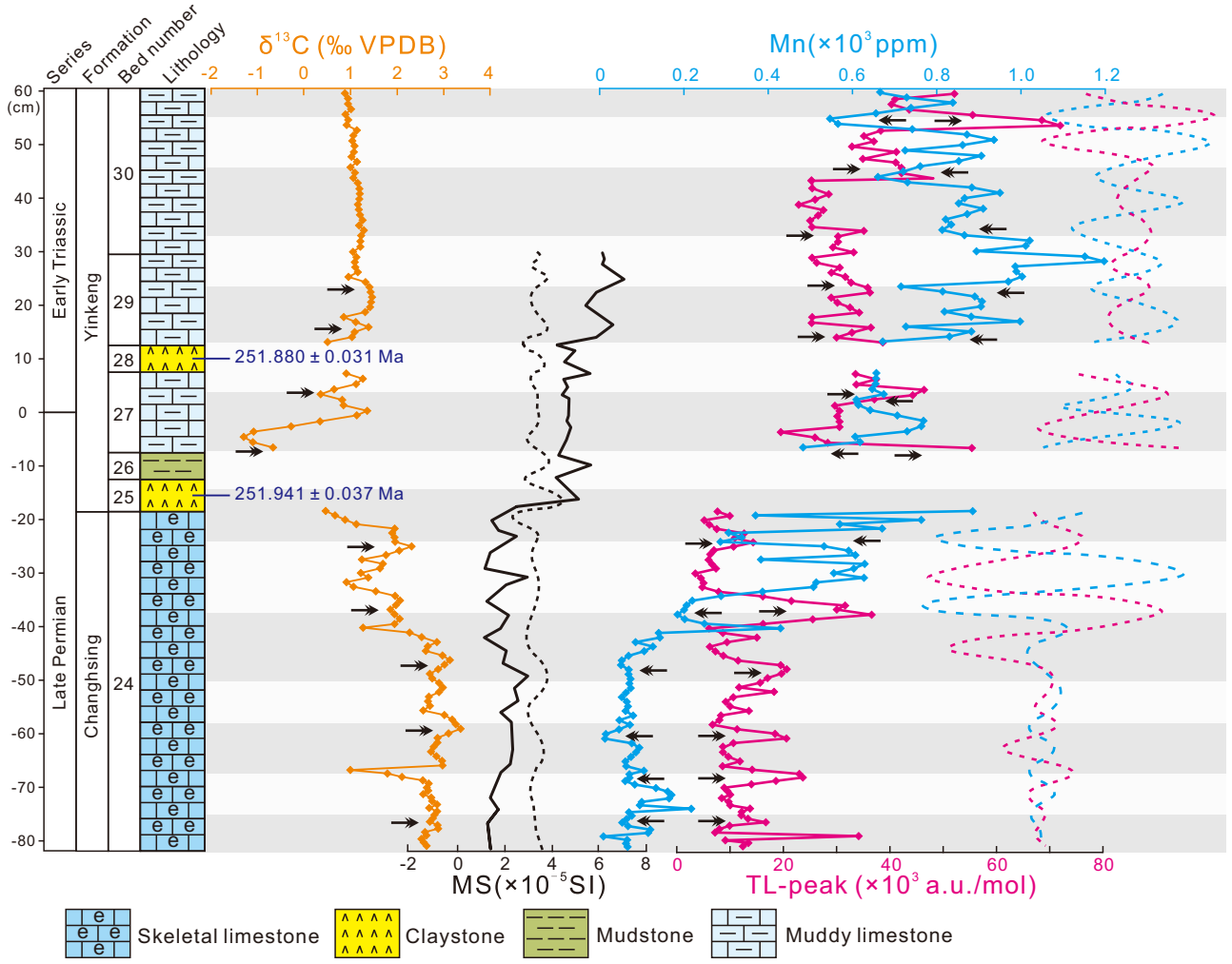
Series
Formation
Bed number
Lithology
δ13C (‰ VPDB)
Mn(×10³ppm)
Early Triassic
Late Permian
Yinkeng
Changhsing
251.880 ± 0.031 Ma
251.941 ± 0.037 Ma
MS(×10⁻⁵SI)
TL-peak (×10³ a.u./mol)
Skeletal limestone
Claystone
Mudstone
Muddy limestone

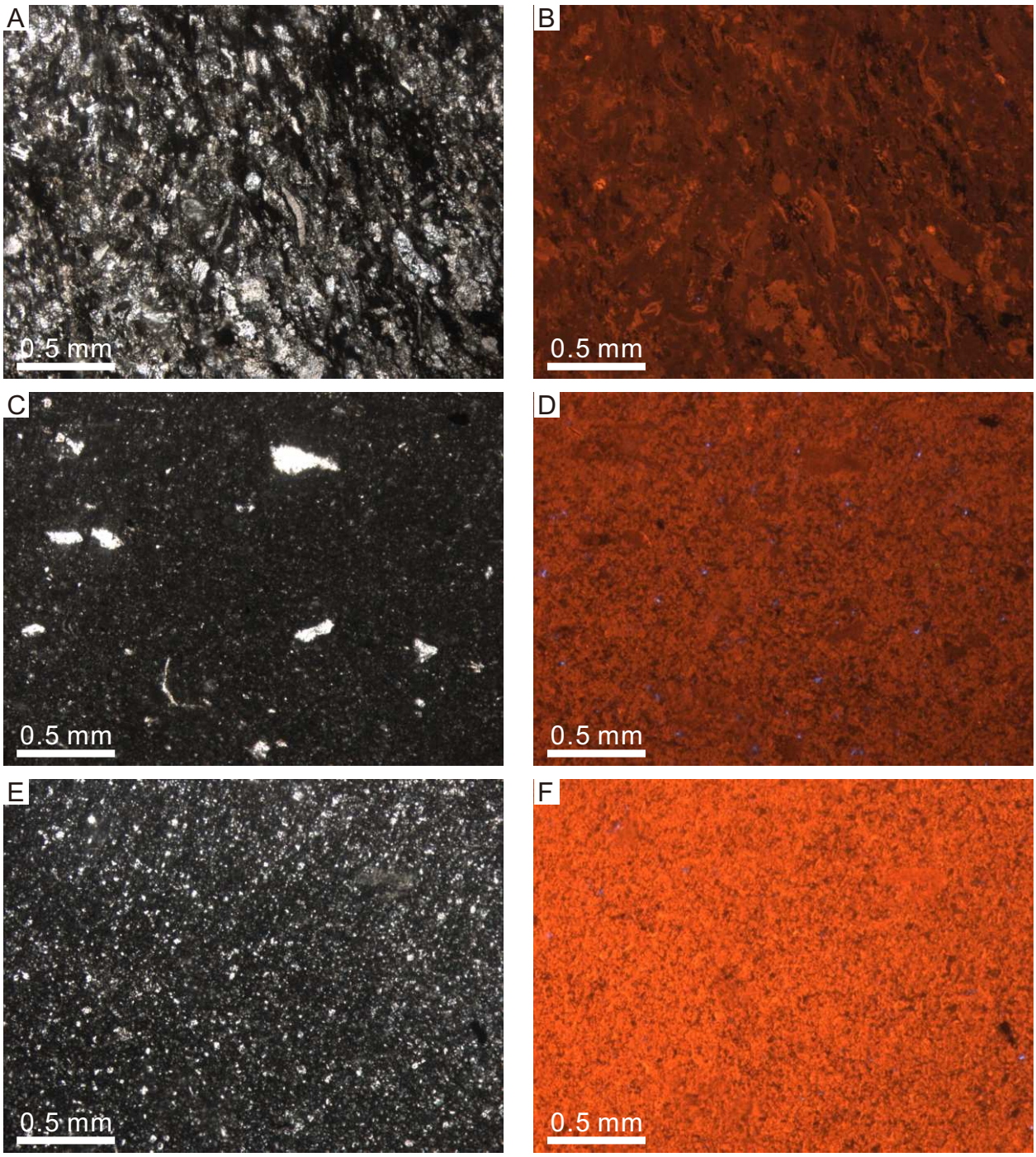
A
0.5 mm
B
0.5 mm
C
0.5 mm
D
0.5 mm
E
0.5 mm
F
0.5 mm

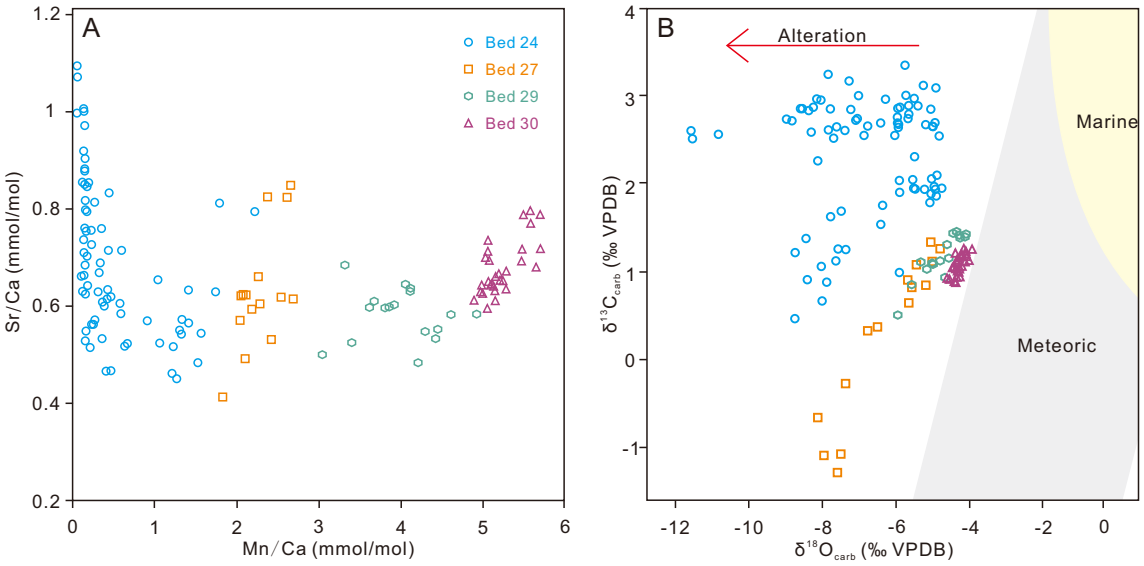
A
Bed 24
Bed 27
Bed 29
Bed 30
Sr/Ca (mmol/mol)
Mn/Ca (mmol/mol)
B
Alteration
Marine
Meteoric
δ13Ccarb (‰ VPDB)
δ18Ocarb (‰ VPDB)

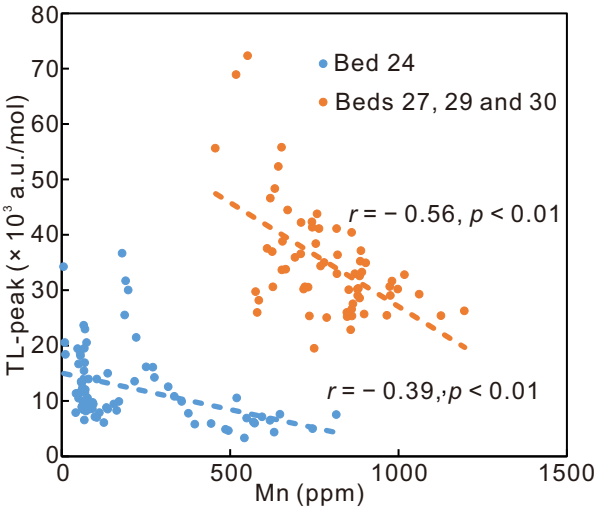
80
70
60
50
40
30
20
10
0
TL-peak (× 10³ a.u./mol)
0
500
1000
1500
Mn (ppm)
Bed 24
Beds 27, 29 and 30
r = − 0.56, p < 0.01
r = − 0.39, p < 0.01

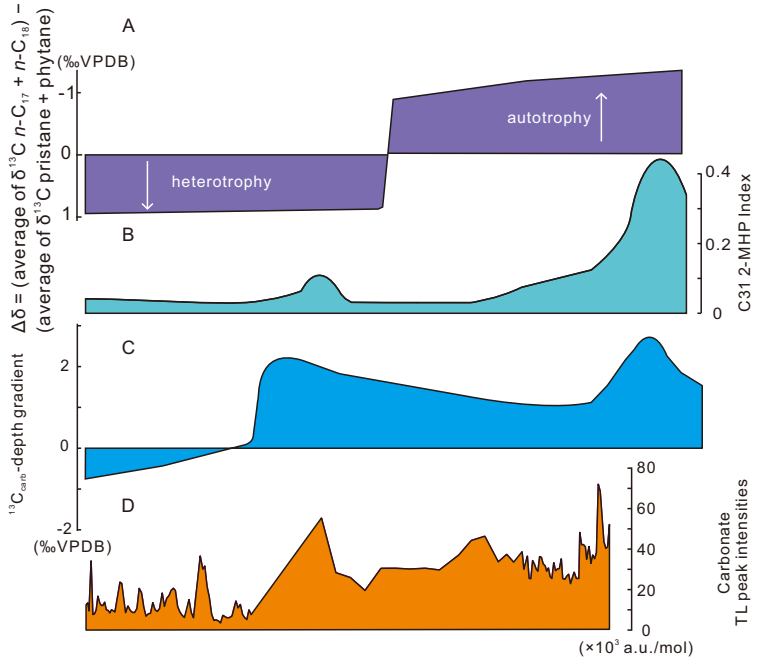

Clarkina yini	*C. m*	*H. chan*	*H. parv*	*I. st*	*Isarcicella isarcica*
Permian			Triassic		